Iron, Copper, and Nickel Behavior in Buffered, Neutral Aluminum Chloride:1-Methyl-3-ethylimidazolium Chloride Molten Salt

Stephen Pye,* Jack Winnick, and Paul A. Kohl****

School of Chemical Engineering, Georgia Institute of Technology, Atlanta, Georgia 30332-0100, USA

ABSTRACT

Iron, copper, and nickel electrodes were examined as possible metal/metal(II) chloride cathodes for the room temperature sodium/metal chloride battery in a molten salt composed of sodium chloride (NaCl), aluminum chloride ($AlCl_3$), and 1-methyl-3-ethylimidazolium chloride (MEIC). The iron electrode was investigated in basic, neutral-like, and acidic MEIC:$AlCl_3$ melts. The solubility and the kinetics of the reduction of Fe(II) was a function of acidity. In the basic melt, the $FeCl_2$ was soluble; however, its reduction was not observed due to slow kinetics. In the neutral-like and acidic melts, the quasi-reversible reduction of Fe(II) to Fe(0) was observed. The redox potential of copper was approximately 1 V more positive of iron; however, the oxidized copper was soluble in the neutral-like melt, making it unacceptable without a separator. The oxidized and reduced forms of nickel were insoluble and the redox potential was 2.5 V positive of Na/Na^+. The nickel electrode supported a charge density of 3.5 mC/cm^2 at room temperature, suggesting that a high-surface-area electrode would be needed in a practical device.

Introduction

Numerous different technologies continue to be investigated in search of an economical, rechargeable battery. Characteristics such as high specific energy (>200 Wh kg^{-1}) and low cost are two targeted parameters. Sodium-based technologies (*i.e.*, using sodium as the anode) meets the two goals due to sodium's low atomic mass, high standard potential, and availability. One of the current rechargeable sodium battery technologies is the "Zebra" cell, which has a specific energy greater than 130 Wh kg^{-1}.[1] This secondary cell operates at ~250°C and uses a molten chloroaluminate inorganic salt, NaCl:$AlCl_3$, as the electrolyte. At this operating temperature, the Zebra cell contains molten sodium (melting point 98°C) as the anode, a solid separator (sodium β″ alumina), and a solid metal chloride (MCl_2) cathode. The half-cell and full-cell reactions follow

$$\text{Charged} \rightleftarrows \text{Discharged}$$

$$\text{Anode: } 2Na \rightleftarrows 2Na^+ + 2e^- \quad [1]$$

$$\text{Cathode: } MCl_2 + 2e^- \rightleftarrows M + 2Cl^- \quad [2]$$

$$\text{Overall: } MCl_2 + 2Na \rightleftarrows 2NaCl + M \quad [3]$$

Although the sodium/metal chloride battery possesses several favorable characteristics, the system operates at a high temperature and uses a separator which increases cell resistance.

Replacing the high-temperature electrolyte with a low-temperature electrolyte (*e.g.*, room temperature) would have several benefits for a sodium-based secondary cell. For instance, at room temperature, the sodium anode could operate in the solid state, removing the necessity for the separator and thereby reducing cell resistance. In addition, operation near room temperature lessens the thermal management requirements and degradation of materials. The room temperature molten salt in this study consists of sodium chloride (NaCl), aluminum chloride ($AlCl_3$), and 1-methyl-3-ethylimidazolium chloride (MEIC). Chloroaluminate electrolytes consisting of MEIC and $AlCl_3$ demonstrate Lewis acid-based chemistry, as shown in Eq. 4 to 7[2,3]

$$Cl^-(l) + AlCl_3(s) \rightleftarrows AlCl_4^-(l) \quad K = 1.6 \times 10^{19} \quad [4]$$

$$AlCl_4^-(l) + AlCl_3(s) \rightleftarrows Al_2Cl_7^-(l) \quad K = 1.6 \times 10^{3} \quad [5]$$

$$Al_2Cl_7^-(l) + AlCl_3(s) \rightleftarrows Al_3Cl_{10}^-(l) \quad K = 1.0 \times 10^{1} \quad [6]$$

$$AlCl_4^-(l) + AlCl_4^-(l) \rightleftarrows Al_2Cl_7^-(l) + Cl^-(l) \quad K = 1.0 \times 10^{-16} \quad [7]$$

In an acidic melt, the moles of $AlCl_3$ exceed those of MEIC and the dominant species are $Al_2Cl_7^-$, $AlCl_4^-$, and MEI^+. In a basic melt, the moles of MEIC exceed those of $AlCl_3$ and the dominant species are $AlCl_4^-$, Cl^-, and MEI^+. The widest potential window is available in the NaCl-buffered, neutral melts, where excess NaCl is present to buffer the melt.[4]

The anode of a NaCl-buffered, neutral MEIC:$AlCl_3$ would use the plating and stripping of sodium, which has been demonstrated by several investigators.[5,6] To construct a battery analogous to the high-temperature Zebra cell, a metal/metal chloride couple would be used. However, a suitable cathode has not been identified in the NaCl-buffered, neutral MEIC/$AlCl_3$ melt.

Ratnakumar *et al.*[7] examined iron, nickel, and copper in the high-temperature (220°C) neutral NaCl:$AlCl_3$ ($NaAlCl_4$) melt. In Ratnakumar's investigations, the copper redox couple possessed the highest potential *vs.* Na/Na^+ (~3.3 V), but the oxidized copper species were soluble. The iron electrode examined showed the lowest redox potential (~2.3 V *vs.* Na/Na^+) and a coulombic efficiency of less than 100%. The nickel electrode possessed the most favorable characteristics. The reversible nickel/nickel(II) redox couple was ~2.6 V positive of the Na/Na^+ couple. In addition, the nickel couple exhibited very high coulombic efficiencies due to the insolubility of both the reduced and oxidized forms.

In an unbuffered, neutral butylpyridinium chloride (BPC):$AlCl_3$ melt, Laher and Hussey[9] observed precipitation of $FeCl_2$. Likewise, these authors also reported the precipitation of $NiCl_2$ in unbuffered, neutral BPC:$AlCl_3$. Nanjundiah *et al.*[10] obtained similar results with Fe(II) insolubility in BPC:$AlCl_3$ melts ranging from $N = 0.498$ to 0.524 (where N is the mole fraction of $AlCl_3$ in the melt).

In the basic MEIC:$AlCl_3$ melt, Lipsztajn and Osteryoung[8] demonstrated that $FeCl_3$ formed a soluble complex, $FeCl_4^-$. In addition, these authors showed a reversible Fe(II)/Fe(III) couple at approximately 0.3 V in a neutral-like melt (basic melt with a stoichiometric amount of $FeCl_3$ added to consume the free Cl^-). Furthermore, in a similar basic melt, ambient temperature chloroaluminate, organic chloride (BPC:$AlCl_3$), Laher and Hussey[9] report that iron(II), iron(III), and nickel(II) all exist as stable mononuclear, tetrahedral complexes such as $FeCl_4^{2-}$, $FeCl_4^-$, and $NiCl_4^{2-}$. These authors report no results of the reduction of metal ions to elemental metal in basic melts.

* Electrochemical Society Student Member.
**Electrochemical Society Active Member.

In the acidic MEIC:$AlCl_3$ melt containing $FeCl_3$, Lipsztajn and Osteryoung[8] reported iron deposition at 0.4 V and the location of the Fe(II)/Fe(III) couple at 1.7 V (*i.e.*, a positive shift relative to the Fe(II)/Fe(III) couple in the basic MEIC:$AlCl_3$ melt). Nanjundiah *et al.*[10] also observed the plating and stripping of iron at a glassy carbon electrode in an acidic BPC:$AlCl_3$ melt containing Fe(II). Pitner *et al.*[15] observed the reduction of a soluble Ni(II) species in the acidic MEIC:$AlCl_3$ melt. A recent study by Dent *et al.*[11] provides data for the coordination environment of metal ions in acidic ambient temperature chloroaluminate organic salts. On the basis of extended x-ray absorption fine structure (EXAFS) data in acidic MEIC:$AlCl_3$ melts containing metal(II) ions, Dent *et al.* suggested that metal (II) species exhibit complexes of the general type $[M(AlCl_4)_3]$. For example, they demonstrated models which agree with the structures of $[Mn(AlCl_4)_3]^-$, $[Co(AlCl_4)_3]^-$, and $[Ni(AlCl_4)_3]^-$.[11] Furthermore, these authors stated that their preliminary results with Fe(II) suggest the same behavior as seen with Mn, Co, and Ni (*i.e.*, $[Fe(AlCl_4)_3]^-$).

We have examined the possibility of a metal/metal chloride couple in the basic and buffered neutral MEIC:$AlCl_3$ melt. Buffering was accomplished by use of NaCl or a metal chloride.

Experimental

Due to the sensitivity of all chemical agents to H_2O and O_2 contamination, the experiments were performed in an inert atmospheric glove box (Vacuum Atmospheres Company) in which H_2O and O_2 levels were each maintained below 10 ppm. Electrochemical experiments were performed with an EG&G Princeton Applied Research Model 263A potentiostat/galvanostat controlled by a personal computer equipped with EG&G M270 software. All electrochemical experiments were performed in a conventional three-electrode glass cell. Working electrodes were either disk or cylindrical (*i.e.*, wire) electrodes. Tungsten disk electrodes were formed by sealing 1 mm diam tungsten wires in borosilicate glass and cutting and polishing the glass/wire electrode such that a disk was formed. Copper and iron disk electrodes were formed by sealing 1 mm diam wires in borosilicate glass tubing with epoxy. The copper and iron disk electrodes were cut and polished to produce disk electrodes. Counterelectrodes consisted of either coiled 0.5 mm diam platinum wires or 1 mm diam aluminum wires. The reference electrode was a 0.5 mm diam aluminum (Alfa, 99.999%) wire immersed in a $N = 0.6$ MEIC:$AlCl_3$ melt contained in a fritted borosilicate glass tube (where N is the mole fraction of $AlCl_3$).

MEIC and $AlCl_3$ were prepared as previously reported.[12] NaCl (Aldrich 99.999%) was heated under vacuum to remove any water present. NaCl-buffered, neutral melts were prepared by adding a 100% excess of NaCl to an acidic ($N = 0.55$) melt. Then the mole fractions of the dominant species were 0.50 $AlCl_4^-$, 0.41 MEI^+, and 0.09 Na^+.

Results and Discussion

The effect of Lewis acidity on the electrochemical behavior of iron was studied in basic, neutral-like, and acidic electrolytes. Cyclic voltammograms were obtained with tungsten and iron working electrodes in the basic melt. The chloride-containing species in the basic melt are primarily Cl^- and $AlCl_4^-$. Previous investigations have shown that the iron(II) existed in the melt as a soluble mononuclear, tetrahedral chloride complex (*i.e.*, as $FeCl_4^{2-}$).[9] To study the behavior of Fe(II) in the basic melt, 0.29 m*M* $FeCl_2$ was added to a basic MEIC:$AlCl_3$ ($N = 0.48$) melt, which contained 11 m*M* free chloride, Cl^-. The solid $FeCl_2$ dissolved in the basic melt as $FeCl_4^{2-}$. The cyclic voltammogram at a tungsten electrode is shown in Fig. 1. The initial potential for the cyclic voltammogram was 0 V, and the initial scan direction was toward positive potentials, to a potential limit of 0.9 V, curve A. An anodic peak of 0.7 mA/cm^2 was observed at 0.3 V due to the oxidation of 10 m*M* $FeCl_4^{2-}$ to $FeCl_4^-$. The oxidation peak at 0.3 V and the reduction peak at 0.2 V were absent in a $FeCl_2$-free,

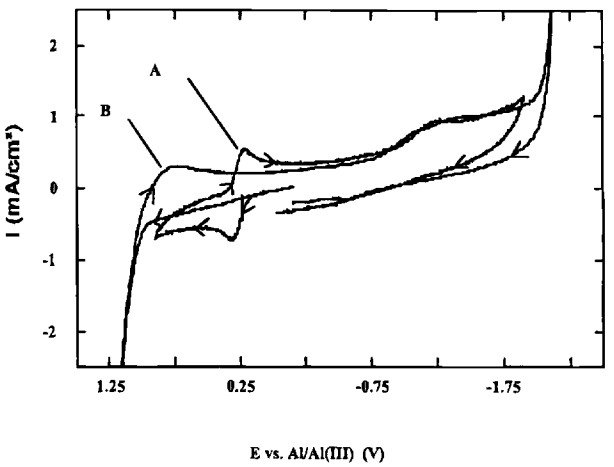

Fig. 1. Cyclic voltammogram at tungsten disk electrode in basic MEIC:$AlCl_3$ ($N = 0.48$) melt at room temperature with (A) 10 m*M* $FeCl_2$ and (B) no $FeCl_2$. Scan rate 100 mV/s and electrode area 7.85 × 10^{-3} cm^2.

basic melt at a tungsten electrode, curve B. The diffusion coefficient for $FeCl_4^{2-}$, assuming a linear-sweep reversible wave was calculated to be 5 × 10^{-7} cm^2/s, in reasonable agreement with the literature value of 2.4 × 10^{-7} cm^2/s.[10] After scan reversal at 0.9 V (curve A), the reduction peak for $FeCl_4^-$ was observed at 0.2 V. It should be noted that there is no change in the acidity of the melt at the electrode surface, because Cl^- was not involved in the electrochemical process. In the absence of $FeCl_4^{2-}$ (curve B), a similar current-voltage behavior was observed in the potential region between 0 and −1.9 V, indicating that the reduction of $FeCl_4^{2-}$ to Fe does not occur in the basic melt. The absence of the reduction of $FeCl_4^{2-}$ to Fe is analogous to the absence of $AlCl_4^-$ reduction to Al due to kinetic limitations in these melts.[13,14]

The voltammographic behavior of an iron disk electrode was examined in the basic ($N = 0.45$) melt. The cyclic voltammogram of the iron electrode is shown in Fig. 2. The voltammogram was started at −0.3 V and scanned in the positive direction to 0.8 V. Three oxidation peaks were observed. The first oxidation peak (I) is believed to signal the oxidation of Fe to Fe(II). Peak II is most likely associated with the oxidation of Fe(II) to Fe(III). The behavior is complicated because the melt at the electrode surface

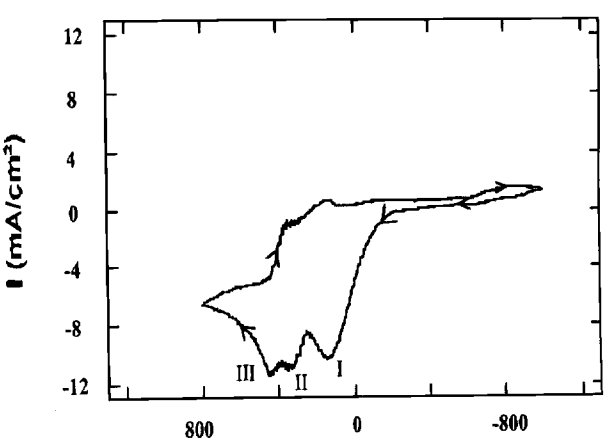

Fig. 2. Cyclic voltammogram of iron disk electrode in basic ($N = 0.45$) MEIC:$AlCl_3$ at room temperature. Scan rate 100 mV/s and electrode area 7.85 × 10^{-3} cm^2.

becomes increasingly acidic as Cl^- is consumed; iron(II) chloride can precipitate under neutral or acidic conditions. On the negative-going scan, following scan reversal toward −1 V, only very small reduction currents were observed. This supports the previous conclusion of slow kinetics for the reduction of Fe(II) to Fe. The small reduction current observed in Fig. 2 are believed to be associated with other species in the melt (as seen with the tungsten disk electrode in Fig. 1).

In summary, an analogy can be made between $AlCl_3$ and $FeCl_2$ with respect to their Lewis-acid and electrochemical behavior. When $AlCl_3$ is added to a basic melt, it complexes with the free chloride and forms the soluble species, $AlCl_4^-$. The ability to scavenge free chloride is also seen with $FeCl_2$, which forms $FeCl_4^{2-}$. Likewise, a similarity exists between the absence of reduction of $AlCl_4^-$ and $FeCl_4^{2-}$ in the basic melt.

A neutral-like MEIC:$AlCl_3$ melt was produced by adding sufficient $FeCl_2$ to a basic melt to consume the excess chloride. In this investigation, the neutral-like MEIC:$AlCl_3$ melt was produced by adding 26 m*M* of $FeCl_2$ to a basic MEIC:$AlCl_3$ (N = 0.45) melt, which contained 30 m*M* free chloride, Cl^-. The melt is neutral-like because it exhibited the voltammetric behavior of a neutral melt where the positive potential limit is 2.2 V (*i.e.*, the $AlCl_4^-$ oxidation to Cl_2), and the negative potential limit was −2.2 V (*i.e*, the MEI^+ reduction). Experiments were conducted at 70°C.

The deposition of Fe(0) was observed by cyclic voltammetry, as shown in Fig. 3. The voltammogram was started at 0.1 V; the initial scan was in the negative direction to a lower potential limit of −1 V. A peak attributed to the deposition of iron was observed at −0.8 V with a current density of 7.9 mA/cm^2. During this reduction, the shiny, metallic appearance of the platinum electrode was darkened by the electrodeposited iron. On the reverse scan, the Fe(0) was stripped from the electrode, as seen by the peak at −0.1 V. Based on the peak separation and charge passed in Fig. 3, the plating and stripping of the Fe/Fe(II) couple is not kinetically or coulombically reversible. For example, the coulombic oxidation/reduction efficiency was 42% (46 mC/cm^6 due to oxidation, 110 mC/cm^2 due to reduction). There was a large peak separation between reduction and oxidation, indicating a kinetically slow process. On the other hand, the plating and stripping of Al/Al(III) in an acidic melt is a kinetically facile process. The plating and stripping of Fe is further supported by comparing the peak potentials of the iron electrode in the NaCl-buffered, neutral MEIC:$AlCl_3$. The codeposition of Fe-Al is a possibility; no elemental analysis of the deposit was performed.

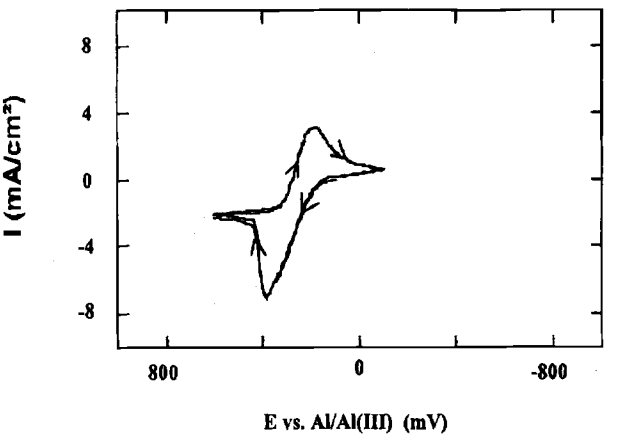

Fig. 4. Cyclic voltammogram at platinum coil electrode in a neutral-like MEIC:$AlCl_3$ melt at 70°C. Scan rate 50 mV/s and electrode area 0.4 cm^2.

The Fe(II)/Fe(III) couple was observed at a platinum electrode in the neutral-like melt, Fig. 4. The voltammogram was started at 0.1 V and the initial scan was in the positive direction; the switching potential was 0.6 V. An oxidation peak was observed at 0.4 V with a current density of 7.1 mA/cm^2. The peak location in Fig. 4 was similar to the peak location in Fig. 1 (the basic melt containing $FeCl_4^{2-}$). The peak potential is not expected to be affected by acidity because Cl^-, the Lewis base, is not involved in the reaction. The reduction of the oxidation products was observed after scan reversal at 0.6 V. The location of the Fe (II)/Fe(III) couple in Fig. 4 is similar to the location of the couple in the previous work by Lipsztajn and Osteryoung using a neutral melt with a small excess of RCl.[8]

To study the behavior of $FeCl_2$ in an acidic melt, $AlCl_3$ was added to the room temperature, neutral-like MEIC:$AlCl_3$ melt containing 26 m*M* $FeCl_2$, forming an acidic (N = 0.55) melt. A platinum coil (area 0.4 cm^2) was used as the working electrode. The cyclic voltammogram shown in Fig. 5 was started at 1.2 V; the initial scan direction was negative, to a potential limit of 0.2 V. This negative limit was chosen positive of the reduction of Al(III) to Al which occurs at 0 V. A reduction current due to the reduction of Fe(II) to Fe was observed negative of 0.5 V, which was absent in a $FeCl_2$-free acidic melt at an inert electrode. On the reverse scan, an oxidation peak was observed at about 0.8 V, which was due to stripping of the plated iron. In addition, the shiny platinum appearance

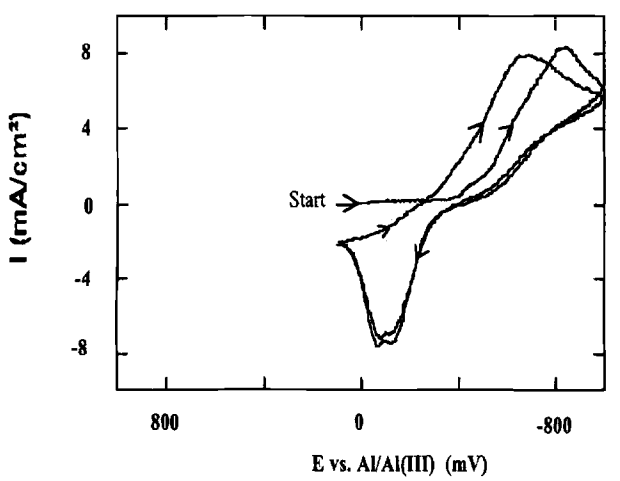

Fig. 3. Cyclic voltammogram at platinum coil electrode in a neutral-like MEIC:$AlCl_3$ melt at 70°C. Scan rate 50 mV/s and electrode area 0.4 cm^2.

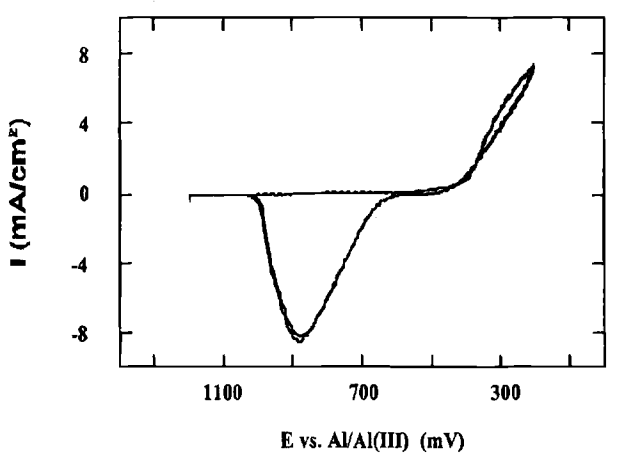

Fig. 5. Cyclic voltammogram at platinum coil electrode in acidic (N = 0.55) MEIC:$AlCl_3$ melt with 26 m*M* $FeCl_2$ at room temperature. Scan rate 50 mV/s and electrode area 0.4 cm^2.

was dark after reduction. Following the oxidation process, the electrode returned to a metallic, shiny appearance. The peak separation for the oxidation and reduction processes was large, like that in the neutral melt. The reduction and oxidation current densities were well within the range of those needed for battery applications.

The coulombic oxidation/reduction efficiency for the plating and stripping process was 100% (34 mC/cm^2 oxidation and 34 mC/cm^2 reduction). This value is significantly higher than observed in the neutral-like, MEIC:$AlCl_3$ melt (46%). The ability to recover all the plated iron suggests that there were no significant parasitic reactions occurring between the plated Fe and the melt. The plating and stripping of Fe was shifted toward more positive potentials compared with the neutral-like MEIC:$AlCl_3$ melt, as would be expected from the higher acidity. Other researchers have observed a similar phenomenon with the shifting of the Fe(II)/Fe(III) couple as the melt acidity became more acidic.[10]

In summary, the plating/stripping of Fe/Fe(II) was observed at 0.3 and 0.8 V, respectively. This is in agreement with the work of Lipsztajn and Osteryoung, who observed Fe(0) deposition at approximately 0.4 V in a "neutral acidic" melt (*i.e*, "neutral" + small excess of $AlCl_3$ at a tungsten electrode at a temperature of 32°C).[8]

The performance of a charged cathode ($FeCl_2$ on a Fe substrate) in a NaCl-buffered, neutral MEIC:$AlCl_3$ melt was investigated using cyclic voltammetry, Fig. 6. The voltammogram was started at −0.3 V and scanned in the negative potential direction to −2.0 V. The first peak (I) at approximately −1 V was due to the reduction of $FeCl_2$ to Fe which covered the electrode. The next reduction peak (II) at −2 V was the reduction of the melt (the negative potential limit of the electrolyte).

During the reduction of $FeCl_2$ (peak I), the melt near the electrode became basic because of the release of Cl^-. Since the melt is saturated with NaCl, the release of chloride may result in the precipitation of NaCl. On the reverse scan, the first oxidation peak (III) at 0 V is attributed to the oxidation of the iron electrode. The decay in the current following peak III is most likely due to passivation of the surface by coating with iron chloride. A small oxidation peak can be seen in Fig. 6 at *ca.* 0.5 V, which may due to the oxidation of iron(II) chloride to iron(III) chloride. The potential for this oxidation peak is similar to that for the oxidation of soluble iron(II) in the neutral-like melt, Fig. 4. Passivation of the electrode could account for the small magnitude of the current. The second oxidation (IV) at 2 V is the positive potential limit of the melt. The potential window of this melt is the same as the neutral-like melt.

The peak current for the oxidation of the iron electrode is low (<5 mA/cm^2), consistent with a passivation phenomenon. The passivation appears to be associated with the formation of $FeCl_2$(s) on the electrode surface. The location of the Fe/Fe(II) peaks in Fig. 6 (the NaCl-buffered melt) was consistent with the location of stripping/plating of Fe/Fe(II) in the neutral-like melt. The nature of the irreversibility (exact electron transfer or chemical step) was not investigated. The Fe/Fe(II) peak separation in Fig. 6 is larger than the peak separation in the high-temperature 220°C NaCl:$AlCl_3$ melt, in which the Fe/Fe(II) couple was more reversible. The small shoulder after peak III at 0.7 V may be due to the oxidation of Fe(II) to Fe(III). The oxidation current identified by IV is the positive limit of the melt.

A previous investigation in an equimolar NaCl:$AlCl_3$ melt at 220°C showed that the copper/copper(II) chloride couple has a more positive redox potential (*e.g.*, 0.5 V) than the iron/iron(II) chloride couple.[7] However, the oxidized form of copper was soluble, an undesirable property for a battery without a separator. In this investigation, the copper/copper chloride couple was investigated in the NaCl-buffered, neutral MEIC:$AlCl_3$, Fig. 7. The voltammogram was started at 0.5 V, and the initial scan direction was toward the positive potential limit of 1.5 V. A steeply rising oxidation current was observed for the copper disk electrode with currents in excess of 300 mA/cm^2. The large oxidation current in the melt is in contrast to the oxidation current density of the iron electrode in the NaCl-buffered, neutral melt, where the current density was lower due to precipitation of the products on the electrode surface. The lack of passivation suggests that the copper ions are soluble. On scan reversal in Fig. 7, a broad reduction current curve in peak currents in the range of 100 mA/cm^2 was observed. The current was due to the reduction of copper ions formed during oxidation. Both the oxidation currents and the reduction current seen in Fig. 7 were absent at an inert tungsten disk electrode in the same melt.

The current-time behavior was quantified with chronoamperometry. The experiment consisted of a double-step chronoamperogram with a potential step to 0.90 V (oxidation of copper) for 15 s followed by potential step to 0.35 V (reduction of copper ions) for 15 s. The coulombs measured during oxidation were 390 mC/cm^2; the coulombs measured during reduction were 240 mC/cm^2. The ratio of the reduction coulombs to oxidation coulombs

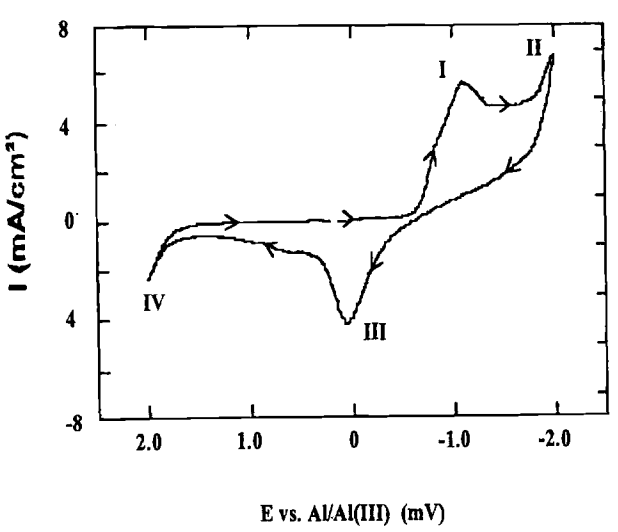

Fig. 6. Cyclic voltammogram at iron/iron(II) chloride wire electrode in NaCl-buffered, neutral MEIC:$AlCl_3$ melt at room temperature. Scan rate 100 mV/s and electrode area 0.071 cm^2.

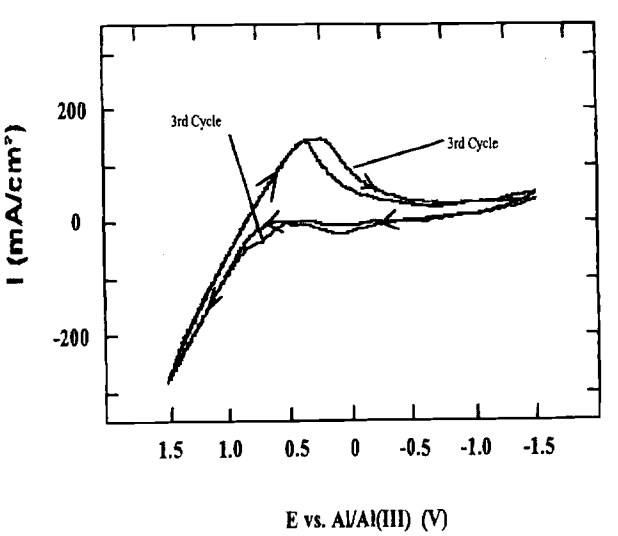

Fig. 7. Cyclic voltammogram consisting of three cycles of a copper disk electrode in NaCl-buffered, neutral MEIC:$AlCl_3$ at room temperature. Scan rate 1 V/s and electrode area 7.85 × 10^{-3} cm^2.

was 0.61; the theoretical value for a diffusion-controlled process is 0.59. Additional chronoamperograms were performed with delay times from 0 to 10 min between the oxidation and reduction potential steps. The reduction/oxidation coulombic efficiency decreases drastically with delay time (*e.g.*, 62% for no time delay to 13% for a time delay of 1 min, 4% for a time delay of 5 min, to 2% for a time delay of 10 min). In summary, this work showed a similarity between the behavior of the copper electrode in the NaCl-buffered, neutral MEIC:$AlCl_3$ (this work) and the inorganic high-temperature neutral NaCl:$AlCl_3$ melt.[7] In both melts, the copper ions in the NaCl-buffered, neutral MEIC:$AlCl_3$ indicated that copper could not be used as a cathode material without a separator.

A study of the behavior of a Ni electrode in the equimolar NaCl:$AlCl_3$ melt at 220°C showed that the nickel/nickel(II) couple had a more positive redox potential than the iron system and formed an insoluble product during oxidation.[7] Both of these features are desirable in a secondary cell. The electrochemical behavior of a nickel wire was examined in the NaCl-buffered, neutral MEIC:$AlCl_3$ melt at 20, 70, 150, and 220°C at three different scan rates (10, 100, and 1000 mV/s).

Figure 8 shows a voltammogram of a nickel electrode at 20°C at a scan rate of 100 mV/s. The scan was started at 0.5 V, and the initial sweep was to −0.5 V. Upon scan reversal, the oxidation peak for Ni to Ni(II) was seen at approximately 0.7 V. The oxidation current density was low because of the formation of $NiCl_2$(s) on the surface; the melt at the electrode surface became acidic during the formation of $NiCl_2$. Upon scan reversal, the reduction of Ni (II) to Ni was observed with a cathodic peak at −0.2 V.

Figure 9a shows a voltammogram of nickel wire electrode at 70°C at a scan rate of 100 mV/s. The negative-going scan was reversed at −0.2 V. On scan reversal to 1.0 V, oxidation of nickel to nickel(II) was observed at 0.8 V. On the next negative-going scan, two cathodic peaks of similar current densities were seen at approximately 0.25 and 0 V, both associated with the reduction of the solid $NiCl_2$ layer. Chemical analysis of the reduction products was not performed. For battery applications, the first cathodic peak (at more positive potentials) is the one of interest. It has been shown that even in acidic melts, nickel metal (not a metal alloy) can be produced.[15] The comparison of the reduction processes at 20°C (Fig. 8), 70°C (Fig. 9a), 150°C (Fig. 9b), and 220°C (Fig. 9c) shows that the current density and total change increase with temperature. In contrast to Fig. 9c, the cyclic voltammograms of nickel in the 220°C neutral NaCl:$AlCl_3$ melt[7] were sharp and did not contain multiple reduction peaks. The difference between the two melts that may cause this difference in reduction behavior is not understood at this time. During the oxidation and reduction processes, the melt near the electrode undergoes a constant change in acidity as chloride is consumed and released by the metal. During oxidation, the passivation of the electrode consumes chloride, and the melt has a tendency to become acidic near the electrode.

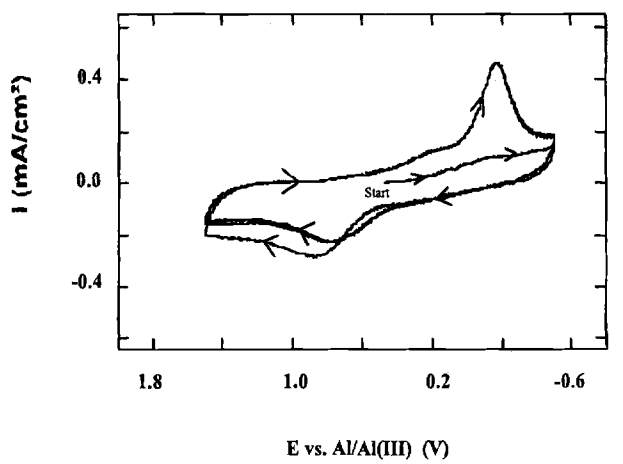

Fig. 8. Cyclic voltammogram consisting of three cycles of a nickel wire electrode in NaCl-buffered, neutral MEIC:$AlCl_3$ at 20°C. Scan rate 100 mV/s and electrode area 0.32 cm^2.

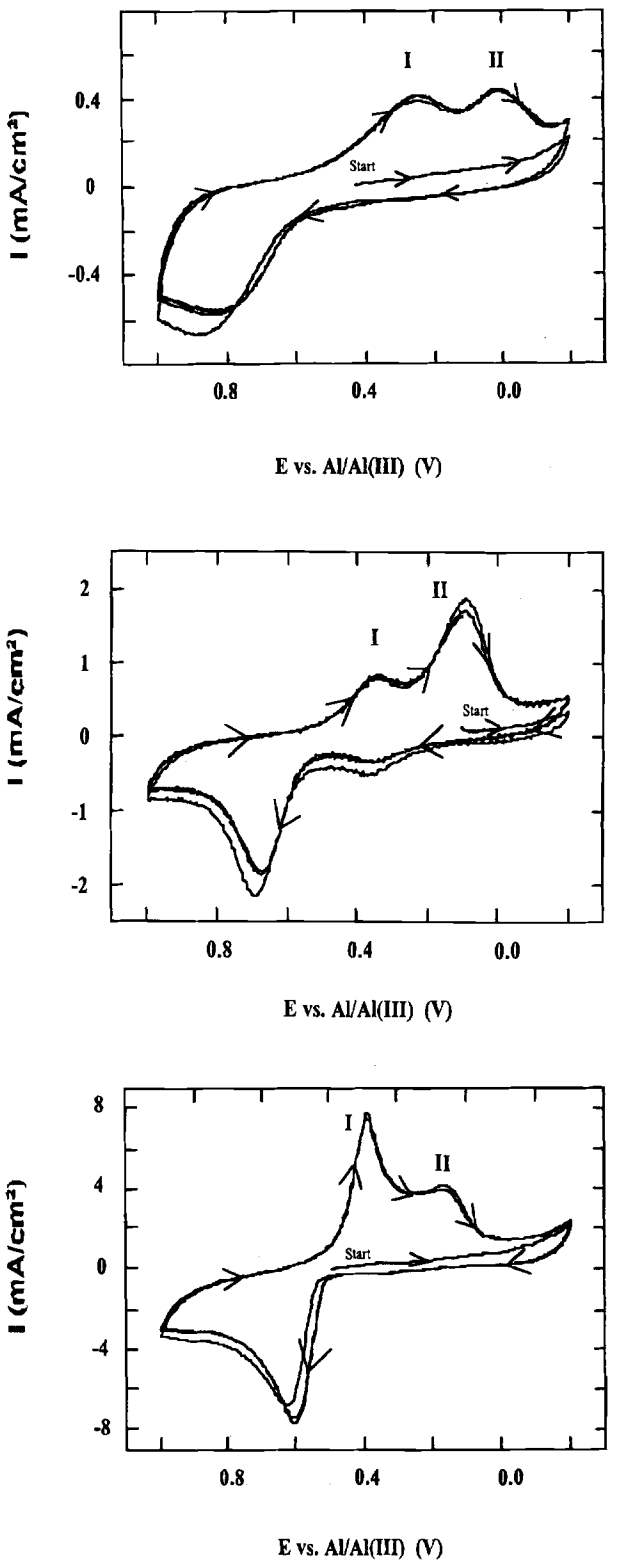

Fig. 9. Cyclic voltammogram consisting of three cycles of a nickel wire electrode in NaCl-buffered, neutral MEIC:$AlCl_3$ at (a, top) 70, (b, middle) 150, and (c, bottom) 220°C. Scan rate 100 mV/s and electrode area 0.32 cm^2.

Table I. Peak separations for the Ni/$NiCl_2$ electrode. Reversible values for a two-electron process: 28 mV for T = 20°C, 33 mV for T = 70°C, 40 mV for T = 150°C, and 47 mV for T = 220°C.

Scan rate (mV/s)	20°C E_p-$E_{p/2}$ (mV)	70°C E_p-$E_{p/2}$ (mV)	150°C E_p-$E_{p/2}$ (mV)	220°C E_p-$E_{p/2}$ (mV)
10	168	108	44	46
100	284	164	72	56
1000	344	317	126	102

For a reversible system, the difference in the peak potential, E_p, and the half-peak potential, $E_{p/2}$, equals 2.2 RT/nF. Assuming a two-electron process, this corresponds to a potential difference of 28, 33, 40, and 47 mV for reversible waves at temperatures of 20, 70, 150, and 220°C, respectively. The experimental anodic data from cyclic voltammetry are listed in Table I. The dependence of the anodic E_p-$E_{p/2}$ on the scan rate was consistent with a quasi-reversible process (*i.e.*, a reversible process is independent of the scan rate). The quasi-reversible system approaches a reversible system at slow scan rates and at high temperatures. In fact, the potential difference at 220°C and 10 mV/s was virtually reversible (46 mV *vs.* the theoretical 47 mV). At higher scan rates and lower temperatures more irreversible behavior is observed.

The anodic charge density *vs.* scan rate data for the cyclic voltammograms performed at varying temperatures are summarized in Table II. The charge increased with increasing temperatures; this trend was consistent with an increasing diffusion coefficient and/or a more porous passivation layer. In addition, the reaction became more reversible as the temperature increased. The charge density also increased as the scan rate decreased; this was most likely due to the longer oxidation times accompanying the slower scan rates. Assuming that the passivation layer was $NiCl_2$, the charge densities in Table II corresponded to solid layers in the range 0.01 to 0.1 μm thick, assuming the density of $NiCl_2$ was that of the bulk material. In summary, the maximum charge density, on a real-surface-area basis, was projected to be about 3.5 mC/cm^2 at 20°C, suggesting a high-surface-area cathode is needed for a viable cell.

Summary

Iron, copper, and nickel were investigated as cathodes in molten organic chloride salt batteries. The iron electrode was investigated in the basic, neutral-like, and acidic MEIC:$AlCl_3$ melts. The investigation of the iron electrode in the sodium-free melts showed that the solubility and the kinetics of the reduction of Fe(II) was a function of acidity. In the basic melt, the Fe(II)/Fe(III) couple was kinetically more facile in the basic melt. In the neutral-like and acidic melts, the kinetically limited reduction of Fe(II) to Fe(0) was observed.

All three metal electrodes were examined in the NaCl-buffered, neutral MEIC:$AlCl_3$ melt. The potential of the iron redox couple was more negative than desired (low battery voltage). Copper exhibited a redox couple at more positive potentials than iron, by about 1 V; however, the oxidized copper species was soluble in the melt. A solid-solid redox couple is desirable so that a battery separator would not be needed. Thus, the copper electrode was viewed as unsatisfactory. In contrast, the nickel system provided a solid-solid redox couple with the formation of nickel chloride at potentials 2.5 V positive of Na/Na^+. The charge density for the nickel electrode was 3.5 mC/cm^2 at room temperature, suggesting that an increase in electrode area is needed for a viable cell.

Table II. Anodic charge density *vs.* scan rate plot for nickel wire electrode in NaCl buffered, neutral MEIC:$AlCl_3$.[a]

Scan rate (mV/s)	20°C Charge density (mC/cm^2)	70°C Charge density (mC/cm^2)	150°C Charge density (mC/cm^2)	220°C Charge density (mC/cm^2)
10	3.3	3.8	12	56
100	2.1	2.5	6.2	23
1000	1.4	1.5	3.9	12

[a]Electrode area 0.32 cm^2 based on cyclic voltammetry data.

Acknowledgments

The support of the Electric Power Research Institute Transportation Business Unit under Contract No. WO 2415-16 is gratefully acknowledged.

Manuscript submitted Sept. 23, 1996; revised manuscript received Feb. 10, 1997.

REFERENCES

1. R. J. Bones, J. Coetzner, R. C. Galloway, and D. A. Teagle, *This Journal*, **134**, 2379 (1987).
2. C. L. Hussey, in *Chemistry of Nonaqueous Solutions: Current Progress*, G. Mamantov and A. I. Popov, Editors, pp. 227-275, VCH, New York (1994).
3. R. T. Carlin and J. S. Wilkes, *ibid.*, pp. 277-306.
4. T. J. Melton, J. Joyce, J. T. Maloy, J. A. Boon, and J. S. Wilkes, *This Journal*, **137**, 3865 (1990).
5. T. L. Riechel and J. S. Wilkes, *ibid.*, **139**, 977 (1992).
6. C. L. Yu, J. Winnick, and P. A. Kohl, *ibid.*, **138**, 339 (1991); G. E. Gray, P. A. Kohl, and J. Winnick, *ibid.*, **142**, 3636 (1995).
7. B. V. Ratnakumar, S. Di Stefano, and G. Halpert, *This Journal*, **137**, 2991 (1990).
8. M. Lipsztajn and R. A. Osteryoung, *Inorg. Chem.*, **24**, 716 (1985).
9. T. M. Laher and C. L. Hussey, *ibid.*, **21**, 4079 (1982).
10. C. Nanjundiah, K. Shimizu, and R. A. Osteryoung, *This Journal*, **129**, 2474 (1982).
11. A. J. Dent, K. R. Seddon, and T. Welton, *J. Chem. Soc., Chem. Commun.*, **139**, 315 (1990).
12. J. S. Wilkes, J. A. Levisky, R. A. Wilson, and C. L. Hussey, *Inorg. Chem.*, **21**, 1263 (1982).
13. Z. J. Karpinski and R. A. Osteryoung, *ibid.*, **23**, 1491 (1984).
14. C. L. Hussey, T. B. Scheffler, J. S. Wilkes, and A. A. Fannin, Jr., *This Journal*, **133**, 1389 (1986).
15. W. R. Pitner, C. L. Hussey, and G. R. Stafford, *ibid.*, **143**, 130 (1996).